Analytical modelling of resistive wall mode stabilization by rotation in toroidal tokamak plasmas

C J Ham, C G Gimblett and R J Hastie

EURATOM/CCFE Fusion Association, Culham Science Centre, Abingdon, Oxon, OX14 3DB, UK.

E-mail: christopher.ham@ccfe.ac.uk

Abstract. Stabilization of the resitive wall mode (RWM) may allow fusion power to be doubled for a given magnetic field in advanced tokamak operation. Experimental evidence from DIII-D and other machines suggests that plasma rotation can stabilize the RWM. Several authors (Finn 1995 *Phys. Plasmas* **2** 3782, Bondeson and Xie 1997 *Phys. Plasmas* **4** 2081) have constructed analytical cylindrical models for the RWM, but these do not deal with toroidal effects. The framework of Connor *et al.* (Connor *et al.* 1988 *Phys. Fluids* **31** 577) is used to develop ideal plasma analytic models with toroidicity included. Stepped pressure profiles and careful ordering of terms are used to simplify the analysis. First, a current driven kink mode model is developed and a dispersion relation for arbitrary current profile is calculated. Second, the external pressure driven kink mode is similarly investigated as the most important RWM arises from this mode. Using this latter model it is found that the RWM is stabilized by Alfvén continuum damping with rotation levels similar to those seen in experiments. An expression for the stability of the external kink mode for more general current profiles and a resistive wall is derived in the Appendix.

Submitted to: *Plasma Phys. Control. Fusion*

1. Introduction

1.1. Background

The resistive wall mode (RWM) in a tokamak is stable with a perfectly conducting wall at the plasma edge, but is unstable in a non-rotating plasma with no wall. An actual tokamak wall has a finite conductivity, which has the consequence that the mode grows at a rate comparable to τ_w^{-1}, where τ_w is the vertical field diffusion time through the wall. Current tokamaks already operate with pulse lengths much longer than τ_w, as will a potential fusion power plant. Fusion power increases like β^2 [1], where $\beta = 2\mu_0 p_0/B_0^2$ is the ratio of plasma pressure, p_0, to magnetic pressure, and B_0 is the equilibrium magnetic field. Mitigating the RWM could increase the β by around 40%, see Reimerdes *et al.* [2] or Hender *et al.* [3], meaning that fusion power could be approximately doubled. Experimental results, particularly on DIII-D, have indicated that RWMs may be stabilized by the rotation of the plasma, see for example the results of Reimerdes *et al.* [4].

Various models have been developed to investigate stabilization of the RWM assuming a number of different dissipation mechanisms. For example: RWM coupling to a dissipative rational surface [5, 6, 7], Alfvén continuum damping [8], sound wave damping [8, 9], ion Landau damping [10], and precessional drift resonance [11]. It seems that toroidal effects are generally important as discussed, for example, in Betti and Friedberg [9] and Gimblett and Hastie [12]. Toroidal effects have been investigated by numerical simulation, for example in Zheng *et al.* [13] or in Liu *et al.* [14]. Also, Betti [15], using a semi-analytical high β toroidal model for the RWM, analysed the effect of toroidal plasma rotation on the various types of resistive and ideal plasma RWMs.

Cylindrical models of tokamak plasmas have been used to model a large number of phenomena analytically. Toroidal models are generally not tractable analytically and so must be solved numerically. A simple toroidal analytic magnetohydrodynamic (MHD) stability model of a tokamak will be developed here. The model uses the large aspect ratio approximation and assumes a circular plasma cross section. The effect of toroidicity is to couple together the poloidal Fourier harmonics $\exp(im\theta)$, where θ is poloidal angle and m is poloidal mode number. Only the adjacent harmonics will be coupled within this model, so that the m harmonic will be coupled to the $m-1$ and $m+1$ harmonics. Toroidal models of the current driven kink mode and the pressure driven external kink mode will be produced. It is known in a tokamak that the most important RWM is linked to the pressure driven ideal external kink mode. Toroidal effects will be shown to be important for the stabilization of the RWM by bulk plasma rotation.

The analytical treatment has used careful ordering of the terms appearing in the equations. In particular, ranking of terms using certain 'magnifying factors' has been used in deriving the equations.

1.2. Overview

The cylindrical model of Bondeson and Xie [7] will be briefly reviewed first in section 2. This will motivate the toroidal models that follow. Section 3 provides some details of Connor *et al* [16], which will be used to produce the toroidally coupled models. This will allow the coupling to be explicitly analysed. Next, a stepped pressure profile will be used to simplify the model provided in [16]. First, a current driven kink mode can be modelled in a low β ordering. This model will be investigated in section 4. Functions which are normalized solutions to the MHD equations based on an arbitrary current distribution can be used to produce a generic dispersion relation. Second, if a higher β ordering is used it is possible to model the pressure driven kink mode. This model will be used to investigate the effect of bulk plasma rotation on the RWM in section 5 with an ideal inertial plasma response [17] at the resonant layer. Discussion and conclusions follow in section 6. The pressure dependence of the stability of the external kink mode with arbitrary current profile and resistive wall is derived in the Appendix.

2. Cylindrical models

2.1. General dispersion relation

Finn [5, 6] and Bondeson and Xie [7] have developed cylindrical plasma models with resistive walls to model the RWM. The formulation by Bondeson and Xie [7] will be briefly reviewed here. A rational surface, at which $m = nq(r_s)$, where n, m are the toroidal and poloidal mode numbers and $q(r)$ is the safety factor profile, is assumed to lie within the plasma. The plasma is assumed to be ideally conducting outside of this mode rational surface, but other effects must be included in a layer enveloping the mode rational surface. Bondeson and Xie [7] model the perturbed magnetic flux ψ, sufficiently far from this mode rational surface, using marginal force balance

$$\frac{1}{r}\frac{\mathrm{d}}{\mathrm{d}r}\left(r\frac{\mathrm{d}\psi}{\mathrm{d}r}\right) - \frac{m^2}{r^2}\psi - \left(\frac{m\mu_0 J_0'}{rF_0} + \frac{2\mu_0 m^2 B_{\theta 0}^2 p_0'}{B_0^2 r^3 F_0^2}\right)\psi = 0, \tag{1}$$

where $F_0 = (B_{\theta 0}/r)(m - nq)$, $'$ denotes the radial derivative and J_0 and p_0 are the equilibrium current and pressure respectively. B_0 and $B_{\theta 0}$ are the unperturbed toroidal and poloidal magnetic induction respectively, $q = (rB_0)/(R_0 B_{\theta 0})$, R_0 is the major radius, and the permeability of free space is μ_0. The solutions of this equation are matched at the resonant surface and also at the resistive wall, therefore it is solved in three separate radial regions. Bondeson and Xie [7] define two solutions of (1): ψ_0, the solution with no wall and ψ_∞ the solution with a perfectly conducting wall. These solutions are normalized, without loss of generality, so that $\psi_0(r_w) = 1$ and $\psi_\infty'(r_w^-) = -1/r_w$. The solution to the resistive wall problem can be expressed as a linear combination of these two solutions

$$\psi(r) = a\psi_0(r) + b\psi_\infty(r). \tag{2}$$

The boundary condition at the resistive wall can be calculated using the pre-Maxwell equations, and a thin wall approximation [18], to be

$$\Delta'_w \equiv \left[\frac{r\psi'(r)}{\psi(r)}\right]_{r_w} = \gamma\tau_w, \tag{3}$$

where γ is the growth rate of the mode, τ_w is the vertical field diffusion time and

$$[f]_r = \lim_{\epsilon\to 0}\left(f(r+\epsilon) - f(r-\epsilon)\right). \tag{4}$$

Imposing this boundary condition on the solution, (2) determines the ratio a/b so that the solution becomes

$$\psi = a\left(\psi_0 + \gamma\tau_w\psi_\infty\right). \tag{5}$$

These outer solutions are continuous across the resonant layer and the jump in derivative defines

$$\Delta'_s \equiv \left[\frac{r\psi'(r)}{\psi(r)}\right]_{r_s}, \tag{6}$$

where r_s is the location of the resonant surface. Bondeson and Xie [7] then give

$$\Delta'_s = \frac{\delta_0 + \gamma\tau_w\delta_\infty}{\psi_0 + \gamma\tau_w\psi_\infty}, \tag{7}$$

where $\delta_0 = [r_s\psi'_0]_{r_s}$ and $\delta_\infty = [r_s\psi'_\infty]_{r_s}$. In [7] it was noted that $\psi_0(r_s) = 0$ and $\psi_\infty(r_s) = 0$ denote the condition for marginal stability of the ideal kink mode without and with a perfectly conducting wall at r_w, respectively. This follows from Newcomb [19] (Theorem 5 and its corollaries).

Solutions to the perfect and no wall problems for arbitrary current profiles will be used to express the resistive wall problem in a generalized form when toroidal coupling is present.

2.2. Layer physics

Equation (1) is used outside the resonant layer. The solutions to this equation couple the wall mode to the layer. Inside the layer, resistive and other non-ideal effects will be required. The layer will respond differently depending on the physical regime the plasma is in. The ideal layer response will be used here; layer physics and the RWM has been investigated in Ham *et al.* [20]. The ideal layer response, in which inertia is dominant [17] , gives

$$\Delta_s(\gamma) = -\frac{\pi}{\gamma\tau_A}, \tag{8}$$

where τ_A is the Alfvén time at the layer, based on B_0. The dispersion relation is formed by matching the solution inside and outside the layer

$$\Delta_s(\gamma) = \Delta'_s. \tag{9}$$

3. Toroidal problem

3.1. Toroidal coupling outside the resonant layer

In section 2 the model was entirely cylindrical in nature. However, as the RWM in a tokamak is essentially toroidal in nature, toroidal coupling effects should naturally be included in the calculation. It is possible to include toroidal effects by using the model developed by Connor *et al.* [16]. This model is derived from the linearized marginal ideal MHD equations

$$\begin{aligned} \nabla\tilde{p} &= \mathbf{j}\times\mathbf{B_0} + \mathbf{J_0}\times\mathbf{b}, \\ \mu_0\mathbf{j} &= \nabla\times\mathbf{b}, \\ \tilde{p} &= -\boldsymbol{\xi}.\nabla p_0, \\ \mathbf{b} &= \nabla\times(\boldsymbol{\xi}\times\mathbf{B_0}), \end{aligned} \tag{10}$$

which represent marginal force balance, Ampére's law, the equation of state for the perturbed pressure, $\tilde{p}$, and the induction equation respectively. The equilibrium current, $\mathbf{J_0}$, magnetic field, $\mathbf{B_0}$, and plasma pressure, p_0, satisfy $\mathbf{J_0}\times\mathbf{B_0} = \nabla p_0$, $\mathbf{j}$ and $\mathbf{b}$ are the perturbed current and magnetic field respectively and $\boldsymbol{\xi}$ is the plasma displacement.

These MHD equations are Fourier decomposed into poloidal harmonics, as in Connor *et al.* [16]. This produces an infinite set of coupled equations for these poloidal harmonics. A large aspect ratio and circular plasma cross-section are assumed, which reduces the coupling to the immediately adjacent harmonics. The resulting system can be represented schematically as

$$\begin{aligned} L_{m-1}\psi_{m-1} &= K^{m}_{m-1}\psi_m + K^{m+1}_{m-1}\psi_{m+1}, \\ L_m\psi_m &= K^{m-1}_{m}\psi_{m-1} + K^{m+1}_{m}\psi_{m+1}, \\ L_{m+1}\psi_{m+1} &= K^{m-1}_{m+1}\psi_{m-1} + K^{m}_{m+1}\psi_m, \end{aligned} \tag{11}$$

where L and K denote second-order radial differential operators and ψ_i represents the ith harmonic of the perturbed magnetic flux. The exact form of these operators can be found in Appendix A of [16]. There is assumed to be no direct coupling between the $m-1$ and $m+1$ harmonics in the models developed here, so $K^{m+1}_{m-1} \equiv 0 \equiv K^{m-1}_{m+1}$. The coupling between the harmonics is generally driven by the Shafranov shift [21] and the pressure gradient.

Connor *et al.* [16] show that the solution between the rational surfaces in their model is spanned by basis vectors that have the form

$$\boldsymbol{\psi}^i = (\psi^i_{m-1}, \psi^i_m, \psi^i_{m+1}), \tag{12}$$

where $1 \leq i$. An equilibrium with two rational surfaces is modelled using five of these basis functions. The first three are regular at the axis and continuous in value and derivative at each of the rational surfaces. Further basis functions are then required at each of the rational surfaces; these are small solutions in the Newcomb sense [19]. Figure 1 shows the radial structure.

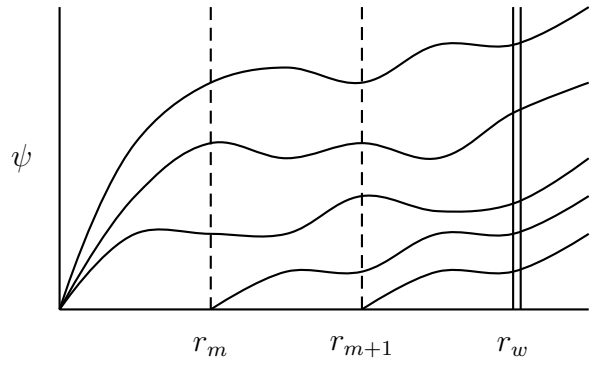

Figure 1. Radial structure of the basis functions, after Connor *et al* [16].

This model is quite complex but a stepped pressure profile will be used to produce analytically tractable models. The pressure step location, r_p, and rational surface are assumed to be very close, so the factor $\kappa \equiv m - nq(r_p)$ is small in the pressure step region and acts as a 'magnifying' term wherever it appears in the denominator of the equations from [16]. The coupling is thus localized to the radius r_p. Terms which are not 'magnified' can be consistently neglected. There is therefore no pressure free coupling in this model.

This model will be used to investigate the current and pressure driven kink modes in sections 4 and 5.

3.2. Toroidal effects inside the resonant layer

In a toroidal configuration it should be noted that there is an enhancement to the plasma inertia in the resonant layer which changes the mode growth rate. The enhancement depends on the collisionality of the plasma. In the MHD fluid regime the inertia is increased by a factor of $m_{\text{eff}} = 1 + 2q^2$ [22] or by $m_{\text{eff}} = 1 + \alpha_0 q^2/\epsilon^{1/2}$, where ϵ is the inverse aspect ratio and α_0 is a constant, in the long mean free path or banana regime [23]. The value of $\alpha_0 = 1.6$ will be used here as given in Rosenbluth and Hinton [24]. There is a further regime where the enhancement is $m_{\text{eff}} = B_0^2/B_{\theta 0}^2$ [25] which holds when $\nu_{ii}/\epsilon \geq \Omega_{\text{rot}}$, where ν_{ii} is the ion-ion collision frequency and Ω_{rot} is the plasma rotation frequency. The effect of this increased plasma inertia is that the Alfvén time is increased by $\sqrt{m_{\text{eff}}}$ and this will be important when the dispersion relation is solved. These effects have been investigated by Shaing [26] using the Fitzpatrick-Aydemir model [27].

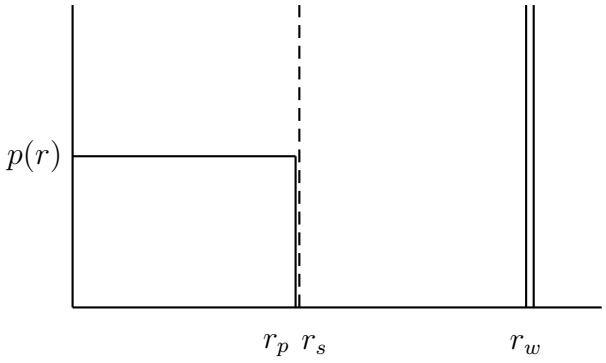

Figure 2. Stepped pressure profile for the kink modes.

4. Current driven kink mode

A stepped pressure profile, shown in figure 2, will be used in this section to model and investigate the stability of a kink mode. This pressure profile means the coupling between the harmonics all occurs at just this one location. It therefore allows the use of arbitrary current profile functions, which can be used to find a dispersion relation.

Definitions of the ordering parameters are required at this point. The ratio of equilibrium plasma pressure to magnetic pressure is

$$\beta_0 = \frac{2p_0\mu_0}{B_0^2}, \tag{13}$$

and the coupling parameter is given by

$$\hat{\beta} = \frac{R_0}{r_p}\frac{2p_0\mu_0 q_0^2}{B_0^2}\frac{m}{m - nq(r_p)} \approx \frac{\beta_0}{\epsilon_p \kappa} \tag{14}$$

where $\epsilon_p = r_p/R_0$ is the inverse aspect ratio.

In this section a low β ordering will be used such that $\beta_0/\epsilon_p \sim \kappa$. In the next section, a higher β ordering will be used such that $\beta_0/\epsilon_p \sim O(\sqrt{\kappa})$. This higher pressure ordering will produce a pressure driven kink mode.

4.1. Equation and boundary conditions

In this current driven kink mode model the coupling occurs just at the pressure step location. This means that the mode can be constructed from solutions to the cylindrical equation

$$\frac{\mathrm{d}}{\mathrm{d}r}\left(r^{1-2l}\frac{\mathrm{d}}{\mathrm{d}r}(r^l\psi_l)\right) = 0, \tag{15}$$

where $l = m-1, m, m+1$. The solutions of this equation are of the form $\psi_l = A_l r^l + B_l r^{-l}$, where A_l, B_l are arbitrary constants. The solutions are matched at the pressure and current steps and at the resonance by jump conditions. The jump in $\psi'_m(r)$ at the resonance defines

$$\Delta'_s \equiv \left[\frac{r\psi'_m(r)}{\psi_m(r)}\right]_{r_s}. \tag{16}$$

The current step jump condition is calculated by integrating the marginal force balance equation from outside the step to inside the step

$$\left[r\frac{\mathrm{d}\psi_m}{\mathrm{d}r}\right]_{r_j} = \frac{2m\psi_m}{J_0(m-nq_0)}\left[J_0\right]_{r_j}, \tag{17}$$

and similarly at other current steps.

The jump conditions at the pressure step are calculated by modelling the pressure profile as

$$p_0(r) = \frac{P_0}{2}\left(1 - \tanh\left(\frac{r-r_p}{\delta r_p}\right)\right), \tag{18}$$

where P_0 is a constant. This represents a step like profile which changes over a width δ. The limit $\delta \to 0$ is taken so that this profile approaches a step function in the sense of generalized function theory [28]. The derivatives of the pressure profile can also be interpreted in this way.

The coupling over the pressure step involves the Shafranov shift, $\Lambda(r)$, which is the solution to

$$\frac{\mathrm{d}^2\Lambda}{\mathrm{d}r^2} = \frac{1}{R_0} - 2\frac{R_0}{r}\frac{\mathrm{d}p_0}{\mathrm{d}r}\frac{q^2}{B_0^2} - \left(\frac{3}{r} + 2q\frac{\mathrm{d}}{\mathrm{d}r}\left(\frac{1}{q}\right)\right)\frac{\mathrm{d}\Lambda}{\mathrm{d}r}, \tag{19}$$

see Connor *et al.* [16].

This equation can be rewritten in the form

$$\frac{\mathrm{d}}{\mathrm{d}r}\left(\frac{r^3B_0^2}{q^2R_0^2}\frac{\mathrm{d}\Lambda}{\mathrm{d}r}\right) = \frac{-2\mu_0 r^2}{R_0}\frac{\mathrm{d}p_0}{\mathrm{d}r} + \frac{r^3B_0^2}{q^2R_0^3}, \tag{20}$$

and then integrated across the pressure step from r_{p-} to r_{p+}. This gives the result

$$\frac{\mathrm{d}\Lambda}{\mathrm{d}r} = \frac{-2\mu_0 R_0 q_p^2}{r_p B_0^2}\frac{P_0}{2}\left(1 - \tanh\left(\frac{r-r_p}{\delta r_p}\right)\right). \tag{21}$$

Differentiating (21) with respect to r then gives

$$r_p\frac{\mathrm{d}^2\Lambda^2}{\mathrm{d}r^2} = \frac{-2\mu_0 R_0 q_p^2}{B_0^2}\frac{\mathrm{d}p_0}{\mathrm{d}r} = \alpha, \tag{22}$$

where $q_p = q(r_p)$ and α is the well known pressure gradient term from ballooning theory [29].

The toroidal coupling equations given in Connor *et al.* [16] are in the form of three second order differential equations. However it will be more convienient here to use an equivalent set of six first order differential equations as given in Martin *et al.* [30]. The equations are multiplied through by δ and then the limit $\delta \to 0$ is taken so that only

terms $O(\alpha)$ are retained. Let $x = (r - r_p)/(\delta r_p)$ and then the equations through the pressure step become

$$\frac{\mathrm{d}\psi_{m-1}}{\mathrm{d}x} = \frac{(m-1)(m-1-nq)}{m-nq}\frac{\lambda}{2}\mathrm{sech}^2(x)\psi_m, \tag{23}$$

$$\frac{\mathrm{d}\psi_m}{\mathrm{d}x} = 0, \tag{24}$$

$$\frac{\mathrm{d}\psi_{m+1}}{\mathrm{d}x} = \frac{-(m+1)(m+1-nq)}{m-nq}\frac{\lambda}{2}\mathrm{sech}^2(x)\psi_m, \tag{25}$$

$$\frac{\mathrm{d}Z_{m-1}}{\mathrm{d}x} = \frac{(1+s)}{m-nq}\frac{\lambda}{2}\mathrm{sech}^2(x)\psi_m, \tag{26}$$

$$\frac{\mathrm{d}Z_m}{\mathrm{d}x} = 0, \tag{27}$$

$$\frac{\mathrm{d}Z_{m+1}}{\mathrm{d}x} = \frac{(1+s)}{m-nq}\frac{\lambda}{2}\mathrm{sech}^2(x)\psi_m. \tag{28}$$

These equations are integrated across the pressure step, from $x \to -\infty$ to $x \to \infty$, to give the final jump conditions over the pressure step

$$[r\psi'_m] = m\hat{\beta}\left((1+s)(\psi_{m+1}-\psi_{m-1}) + \frac{r\psi'_{m+1}}{(m+1)} + \frac{r\psi'_{m-1}}{(m-1)}\right), \tag{29}$$

$$[\psi_m] = 0, \tag{30}$$

$$\left[r\psi'_{m+1}\right] = \frac{(m+1)^2}{m}(1+s)\hat{\beta}\psi_m, \tag{31}$$

$$[\psi_{m+1}] = -\frac{(m+1)}{m}\hat{\beta}\psi_m, \tag{32}$$

$$\left[r\psi'_{m-1}\right] = -\frac{(m-1)^2}{m}(1+s)\hat{\beta}\psi_m, \tag{33}$$

$$[\psi_{m-1}] = -\frac{(m-1)}{m}\hat{\beta}\psi_m, \tag{34}$$

where $s = rq'(r_p)/q(r_p)$ is the magnetic shear. These jump conditions were previously reported in [31]. It should be noted that the RHS of (29) can be shown to be continuous across $r = r_p$, even though all of the constituent parts are, individually, discontinuous. Consequently, (29) is unambiguous. Also note that there are jumps in the $m-1$, (34), and $m+1$, (32), harmonics themselves. These are due to Pfirsch-Schluter current sheets resulting from the pressure step [32].

4.2. Generic current profile

It is possible to find a generic expression for Δ' for the current driven kink mode using the pressure step jump conditions derived above. Bondeson and Xie [7] used a similar technique for the cylinder where they found the form given in (7). The final form of Δ' (see the Appendix for the derivation) is

$$\Delta'_s = \frac{c_0 + \gamma\tau_w c_1 + (\gamma\tau_w)^2 c_2 + (\gamma\tau_w)^3 c_3 + \hat{\beta}^2(d_0 + \gamma\tau_w d_1 + (\gamma\tau_w)^2 d_2 + (\gamma\tau_w)^3 d_3)}{a_0 + \gamma\tau_w a_1 + (\gamma\tau_w)^2 a_2 + (\gamma\tau_w)^3 a_3}, \tag{35}$$

where a_i, c_i, d_i are quantities independent of pressure, details given in the Appendix. The $m+1$ and $m-1$ harmonics are coupled by a $\hat{\beta}^2$ term rather than a $\hat{\beta}$ term.

It is important to note that this model can only be used for current driven instabilities. Although (35) contains the effect of pressure, which causes harmonic coupling, it is not possible to make an ideally stable plasma ideally unstable by increasing pressure in this model; the shape of the current profile would have to change too. This is because $\Delta' \to \infty$ is required for ideal instability, since this implies $\psi_m(r_s) \to 0$, and this does not happen at finite $\hat{\beta}$ in this model. A denominator in (35) which goes to zero at finite $\hat{\beta}$, for example, would be required for this. A different, higher $\hat{\beta}$, ordering will be investigated in section 5 which will allow ideal instability at finite $\hat{\beta}$.

5. Pressure driven kink mode

In a tokamak the most important RWM arises from a pressure driven ideal external kink mode. It has been noted that the model in section 4 cannot produce such an instability. In this section the Connor *et al.* [16] structure will be used to produce a model which exhibits the key features of an ideal toroidal pressure driven kink mode. This is done by adopting a higher pressure ordering so that $\beta_0/\epsilon_p \sim O(\sqrt{\kappa})$ where $\kappa \equiv m - nq(r_p) << 1$ instead of $\beta_0/\epsilon_p \sim O(\kappa)$. The technique of using a magnifying factor is still being used in this section but the $\hat{\beta}$ parameter is ordered differently. The same boundary and jump conditions as used in section 4 will be used here.

5.1. Generic current profile

It is possible to derive an expression for Δ' for the pressure driven kink mode using arbitrary-current functions. The details of this calculation are given in the Appendix. The result has the form

$$\Delta'_s = \frac{a_0 + a_1\gamma\tau_w + a_2(\gamma\tau_w)^2 + a_3(\gamma\tau_w)^3}{b_0 + b_1\gamma\tau_w + b_2(\gamma\tau_w)^2 + b_3(\gamma\tau_w)^3}, \tag{36}$$

where a_i and b_i are quantities dependent on the pressure. In this model it is now possible to drive a stable ideal mode ideally unstable by increasing the pressure alone. The denominator can go to zero so that $\Delta'_s \to \infty$ at finite $\hat{\beta}$ indicating ideal marginal stability. For example, taking the 'no wall' limit ($\tau_w \to 0$) the functional form becomes $\Delta'_s = (e_1 + e_2\hat{\beta}^2)/(e_3(\hat{\beta}^2 - \hat{\beta}^2_{\text{No wall}}))$ or taking the 'perfect wall' limit ($\tau_w \to \infty$) the form is $\Delta'_s = (e_4 + e_5\hat{\beta}^2)/(e_6(\hat{\beta}^2 - \hat{\beta}^2_{\text{Perfect wall}}))$, where e_i are pressure independent quantities. Both of these limits therefore have the required property that $\Delta'_s \to \infty$ at finite $\hat{\beta}$.

This replaces the 'device' employed in the Finn model to introduce an internal resonant surface into a cylindrical calculation in order to attempt the modelling of a toroidal mode. The effects of rotation on (36) will be investigated.

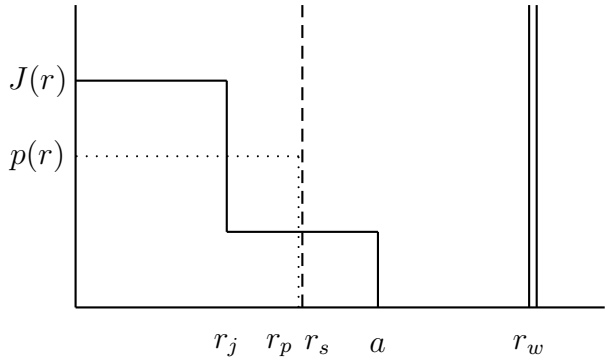

Figure 3. Current and pressure profile for the pressure driven kink mode.

5.2. Specific equilibrium

A specific set of parameters have been chosen to model a typical ideal pressure driven external kink mode with a resistive wall. The current profile is uniform either side of the two steps at $r_j = 0.5$ and $a = 1$. The ratio of the current density for $r_j < r < a$ to the current density for $r < r_j$ is $\zeta = 0.4$. The resistive wall is located at $r_w = 1.15$. The pressure step is at $r_p = 0.9$ and the rational surface just outside at $r_p + \epsilon = 0.905$. A 'cartoon' of the equilibrium is shown in figure 3. The poloidal mode number is $m = 2$. The safety factor profile is flat for $r \leq r_j$ with $q(0) = 1.166$ and monotonically increasing for $r > r_j$ with $q(a) = 2.121$. The full toroidal problem is solved by matching the solutions in each region together using the jump conditions at the pressure and current steps and at the wall. The final dispersion relation has the form of (36), as derived in the Appendix.

The no wall stability limit of this equilibrium is $\hat{\beta} = 2.4574$ and the perfect wall limit is $\hat{\beta} = 7.9254$. Figure 4 shows the behaviour of Δ' with increasing pressure in the no wall and perfect wall cases. The poles can clearly be seen at the no wall and perfect wall pressure limits.

Figure 5 shows how the perfect wall $\hat{\beta}$ limit changes with the position of the perfect wall. Note that for large r_w/a the perfect wall $\hat{\beta}$ limit asymptotes to the no wall limit. If the perfect wall is sufficiently close to the plasma, $r_w < 1.082a$, then the mode is always stable. A similar result is given in Betti [15] but without the region of second stability found there.

The stability of the RWM with rotation can be investigated by giving the plasma a bulk rotation Ω with respect to the wall. The ideal layer response will be assumed for

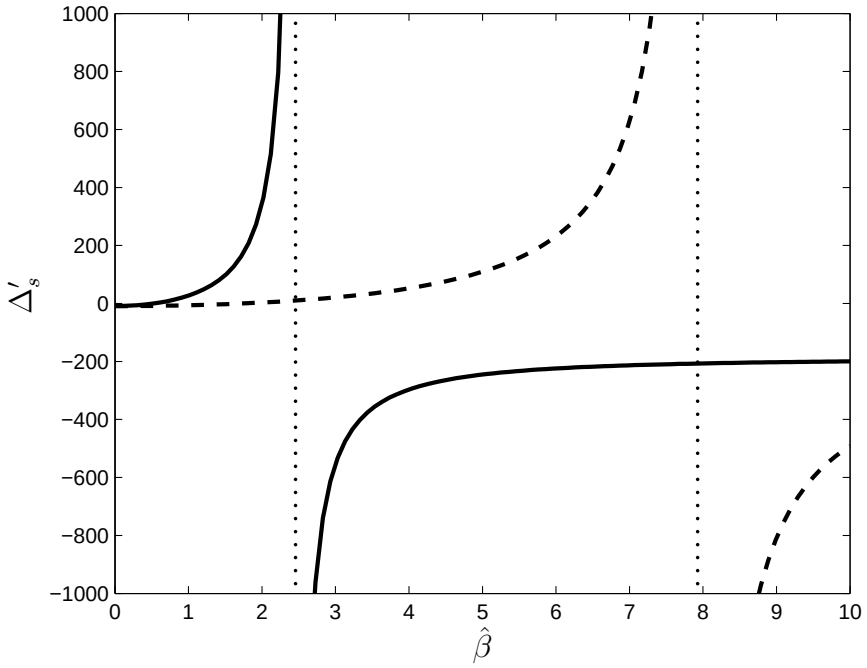

Figure 4. Δ' with increasing pressure, $\hat{\beta}$. The solid line shows the no wall case and the dashed line the perfect wall case. The poles (vertical dotted lines) can clearly be seen at the no wall and perfect wall pressure limits.

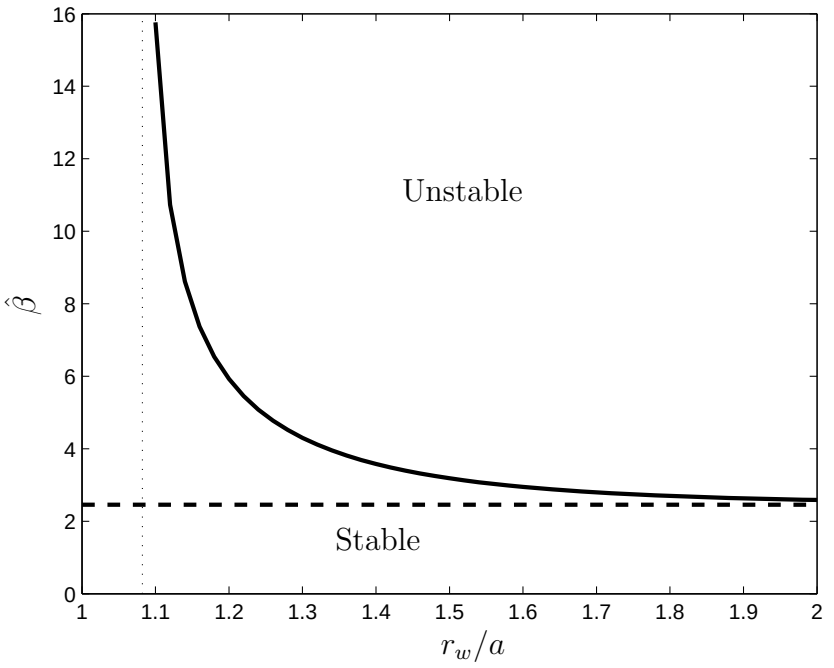

Figure 5. The perfect wall $\hat{\beta}$ limit increases as the wall is moved closer to the plasma. The perfect wall limit approaches the no wall limit for large r_w/a.

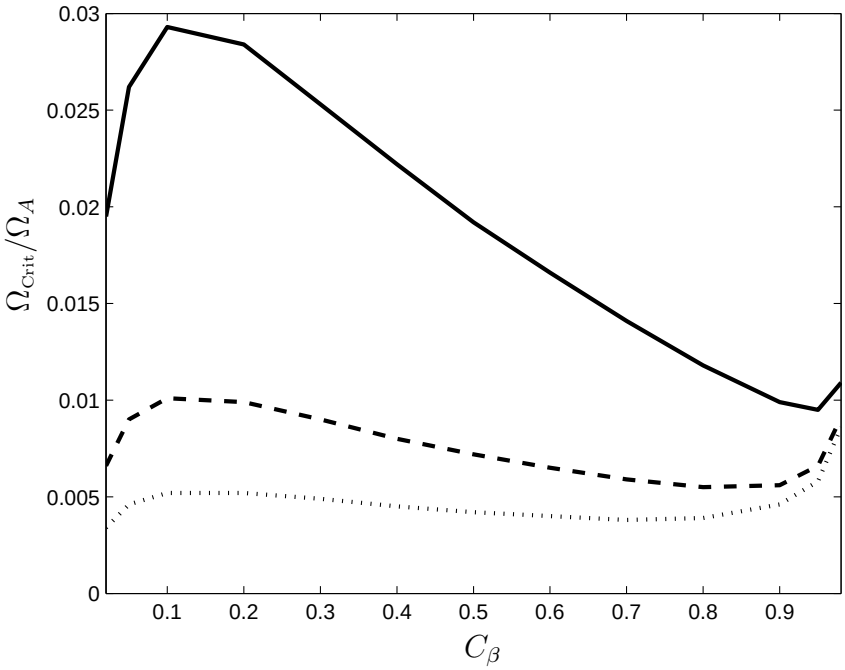

Figure 6. Critical rotation required for stabilization as a proportion of Alfvén rotation is on the y-axis and C_β is on the x-axis. The solid line has no inertial enhancement, the dashed line has $\tau_A^{\rm eff} = 3\tau_A$ and the dotted line has $\tau_A^{\rm eff} = 6\tau_A$.

simplicity. The following dispersion relation is solved

$$\Delta_s' = \Delta_m(\gamma) = -\frac{\pi}{(\gamma - {\rm i}\Omega)\tau_{\rm A}}, \tag{37}$$

and $\tau_w/\tau_A = 14000$ will be used as is typical in DIII-D experiments [2].

In subsection 3.2 it was noted that there is an enhancement to the inertia in a toroidal configuration. This occurs both in the high and low collisionality regimes. The typical DIII-D plasma is in the low collisional or banana regime. The aspect ratio of DIII-D is ~ 3 and the $q = 2$ surface is of interest so that the expected enhancement to the inertia is ~ 9 and the effective Alfvén time is approximately three times longer. If a higher value of q is relevant then the effective Alfvén time could easily be enhanced by a factor ~ 6 ($q \sim 4$). In a typical DIII-D plasma at stabilization of the RWM it is possible that $\nu_{ii}/\epsilon \geq \Omega_{\rm rot}$, which would mean the $B_0^2/B_{\theta 0}^2$ regime is applicable.

Reimerdes *et al.* [2] use the parameter

$$C_\beta = \frac{\beta - \beta_{\rm No\ wall}}{\beta_{\rm Perfect\ wall} - \beta_{\rm No\ wall}}, \tag{38}$$

as a measure of the instability drive where $\beta_{\rm No\ wall}$ is the no wall β limit and $\beta_{\rm Perfect\ wall}$ is the perfect wall β limit. Figure 6 shows the levels of rotation required to stabilize the RWM as C_β increases. This plot can be compared against experimental values. The results given in Reimerdes [2] show the critical rotation for stabilization to be between 0.5% to 1.0% Ω_A at the $q = 2$ surface, which is similar to the levels predicted

here, but these experiments used magnetic braking to slow the plasma. However, later experiments with balanced neutral beams [4, 33] indicate that slower stabilization, at around 0.3% Ω_A, is possible with C_β up to 0.4. This level of experimental critical rotation shows agreement with that predicted here with inertial enhancement. It should be noted that this model does not use fully realistic pressure and current profiles and so agreement with experimental results should be treated with some caution. Betti [15] shows similar results for the rotation required to stabilize the the ideal plasma resistive wall mode with increasing $\hat{\beta}$.

The calculations for figure 6 have been carried out for the no enhancement case and two different values of enhanced inertia, $\tau_A^{\text{eff}} = 3\tau_A$ and $\tau_A^{\text{eff}} = 6\tau_A$. It can be seen from figure 6 that this enhanced inertia reduces the critical rotation required for stabilization of the RWM.

The drive for the instability comes from the pressure. The stabilization mechanism is due to the $m + 1$ harmonic being coupled to the m harmonic which has Alfvén continuum damping available at the resonant layer.

6. Discussion and Conclusions

Cylindrical models of the resistive wall mode were briefly reviewed including the form of Δ' in Bondeson and Xie [7]. In order to generalize this to a toroidal model, work on the coupling of poloidal harmonics, as in Connor *et al.* [16], and the enhancement of plasma inertia in the resonant layer were reviewed [26].

Stepped pressure and current profiles were used with careful ordering of terms to produce 'magnifying factors' thus confining toroidal harmonic coupling to specific radial locations. The resulting jump conditions allowed an analytic expression for Δ' to be found with a low β ordering and with a high β ordering. It was shown that the low β ordering could only produce a current driven mode, not a pressure driven kink mode. The generic form of the current driven kink mode was given.

If a higher β ordering was used, then a pressure driven kink mode could be produced. A generic form of this pressure driven kink mode was derived in the Appendix. The no wall and perfect wall Δ' both contain a $1/(\hat{\beta}^2 - \hat{\beta}^2_{\text{Wall}})$ like pole.

A specific equilibrium was investigated and the required levels of rotation calculated for stabilization at different pressure levels. If an ideal layer response was assumed then the levels of rotation required for stabilization show broad agreement with experimental results. The effect of enhanced inertia in the resonant layer was also included and was shown to reduce the required rotation for stabilization of the RWM.

The critical rotation required for stabilization predicted by numerical codes has similar levels to those seen here [2]. However, to achieve this those codes contained additional parallel viscous damping (to model the effect of ion Landau damping [34]). In this paper it was found that, provided the rotation frequency is low enough to satisfy $\nu_{ii}/\epsilon \geq \Omega$, enhanced neo-classical inertia can achieve similar results, though it has to be noted that the equilibria used here involve step functions in the pressure and current

profiles.

Acknowledgments

It is a pleasure to acknowledge J W Connor and Y Q Liu for useful discussions.

This work was funded by the UK Engineering and Physical Sciences Research Council under grant EP/G003955 and by the European Communities under the contract of association between EURATOM and CCFE. The views and opinions expressed herein do not necessarily reflect those of the European Commission.

Appendix A. Derivation of the functional form of Δ'

If a toroidal plasma with large aspect ratio and circular cross-section is assumed, the central harmonic, m, will be coupled to the adjacent harmonics, $m-1$ and $m+1$. In the case of a pressure step the coupling is provided *only* at the pressure step and it is given by the jump conditions, (29)-(34). This will allow the form of Δ'_s for the external pressure driven kink mode to be derived using functions that can be defined purely from cylindrical calculations. This process will mean that the full pressure dependence of Δ'_s is displayed. It will also allow external pressure driven kink mode dispersion relations to be calculated very efficiently.

It should be noted that the functions and method used here are not the same as the basis functions used by Connor *et al.* [16] which: (i) satisfy the boundary condition as $r \to 0$, (ii) are the solutions of the coupled equations through each Newcomb subinterval, (iii) do not individually satisfy the boundary condition as $r \to \infty$, and (iv) do not individually satisfy the correct jump conditions across the resonant surface.

The functions for the side-band harmonics will be defined first followed by the main harmonic. These functions will be combined to produce the no wall and perfect wall eigenfunctions. They will also be combined together to form a number of triplet basis functions which will be used to construct the RWM eigenfunction. The pressure step jump conditions will be used to determine the amplitudes of the sideband harmonics. The functional form of Δ' for the current driven kink mode and the pressure driven kink mode will then be given.

Appendix A.1. Sideband functions

The sideband harmonics will be calculated by first integrating (1) from just outside the pressure step to $r \to \infty$. These solutions will be labelled $\phi_l^{+0,\infty}(r)$ where $l = m-1, m+1$ and 0 denotes the no wall case and ∞ denotes the perfect wall case. These functions respect the boundary conditions $\phi_l^{+0}(r) \to 0$ as $r \to \infty$ in the no wall case or $\phi(r_w)_l^{+\infty} = 0$ in the perfect wall case. They are also normalized such that $\phi_l^{+0}(r_w) = 1$ and $\phi_l'^{+\infty}(r_w) = -1/r_w$, and so are fully determined.

Next, (1) is integrated from $r = 0$, with boundary condition $\phi_l(0) = 0$ to just inside the pressure step. These solutions are labelled $\phi_l^{-0,\infty}(r)$ and are normalized such that

$\phi_l^{-0,\infty}(r_p) = 1$. These functions are also fully determined. In fact these functions do not reach the wall and are unaffected by it, therefore the perfect wall and no wall functions are the same, and so $\phi_l^{-0}(r) = \phi_l^{-\infty}(r) \equiv \phi_l^{-}(r)$, for $l \equiv m \pm 1$.

The sideband functions are defined as

$$\begin{aligned}\psi_l^{0,\infty}(r) &= \alpha_l^{0,\infty}\phi_l^{-}(r) \quad \text{for} \quad r < r_p,\\ &= \phi_l^{+0,\infty}(r) \quad \text{for} \quad r > r_p,\end{aligned}$$

where $\alpha_l^{0,\infty}$ are to be determined and will in general depend on the pressure.

Appendix A.2. Main harmonic function

The main harmonic is defined, in a similar way to the sideband functions, by integrating (1) from just outside the resonant layer, r_s, to $r \to \infty$ with no wall and a perfect wall. These solutions will be labelled $\phi_m^{+0,\infty}(r)$. They respect the boundary conditions $\phi_m^{+0}(r) \to 0$ as $r \to \infty$ in the no wall case or $\phi(r_w)_m^{+\infty} = 0$ in the perfect wall case and are normalized such that $\phi_m^{+0}(r_w) = 1$ and $\phi_m'^{+\infty}(r_w) = -1/r_w$. These functions are thus fully determined. Again, (1) is integrated from $r = 0$ to just inside the pressure step and normalized such that $\phi_m^{-}(r_p) = 1$.

Finally, the main harmonic function between r_p and r_s will be the sum of two functions. The first will be $\phi_m^{-}(r)$ which will be continued to r_s, and the other will be $\phi^{ps}(r)$, which is defined as $\phi^{ps}(r) = 0$ for $r < r_p$ and for $r > r_s$ and for $r_p < r < r_s$ by integrating (1) from r_p to r_s. It is normalized such that $\phi^{ps}(r_p) = 0$ and $\phi'^{ps}(r_p) = 1$.

The arbitrary-current main harmonic functions can now be defined as

$$\begin{aligned}\psi_m^{0,\infty}(r) &= \alpha_m^{0,\infty}\phi_m^{-}(r) \quad \text{for} \quad r < r_p,\\ &= \alpha_m^{0,\infty}\phi_m^{-}(r) + \alpha_{ps}^{0,\infty}\phi^{ps}(r) \quad \text{for} \quad r_p < r < r_s,\\ &= \phi_m^{+0,\infty}(r) \quad \text{for} \quad r > r_s,\end{aligned}$$

where $\alpha_m^{0,\infty}$ and $\alpha_{ps}^{0,\infty}$ are to be determined and generally depend on the pressure.

Appendix A.3. No wall and perfect wall basis functions

Basis functions consisting of triplets of the functions defined above can now be formed to find the no wall and perfect wall eigenfunctions. The triplet for the no wall problem will be

$$\psi_{m-1}(r) = a_{m-1}\psi_{m-1}^{0}(r), \tag{A.1}$$
$$\psi_{m}(r) \quad = a_{m}\psi_{m}^{0}(r), \tag{A.2}$$
$$\psi_{m+1}(r) = a_{m+1}\psi_{m+1}^{0}(r), \tag{A.3}$$

where $\psi_l^{0,\infty}$ are defined in the section above. The triplet for the perfect wall problem will be

$$\psi_{m-1}(r) = w_{m-1}\psi_{m-1}^{\infty}(r), \tag{A.4}$$
$$\psi_{m}(r) \quad = w_{m}\psi_{m}^{\infty}(r), \tag{A.5}$$
$$\psi_{m+1}(r) = w_{m+1}\psi_{m+1}^{\infty}(r), \tag{A.6}$$

where a_j and w_j, $j = m-1, m, m+1$, are to be determined using the pressure jump conditions.

Appendix A.4. Pressure jump conditions: no wall and perfect wall

The pressure step jump conditions are now used to determine the constants in this system of equations for each of the no wall and perfect wall problems. Using the no wall problem as an example, there are seven undetermined constants, namely a_j, α_j^0 and α_{ps}^0 where $j = m+1, m, m-1$. There are six pressure step jump conditions, but continuity of the m harmonic through the pressure step has already been used, so five remain. There is a further condition requiring the main harmonic to be continuous at r_s. Therefore, there are six conditions left to be satisfied. This will specify the system up to one constant, which can be normalized since it is a linear eigenfunction, so let $a_m = 1$.

The results of the no wall and modified perfect wall problems will be useful for the resistive wall problem. The $\alpha_{m\pm1}^{0,\infty}$ are determined by the sideband jump conditions at the pressure step, (32) and (34), so that

$$\alpha_{m-1}^0 = \frac{(m-1)\hat{\beta}\alpha_m^0 a_m}{m a_{m-1}} + \phi_{m-1}^{+0}(r_p), \tag{A.7}$$

$$\alpha_{m-1}^\infty = \frac{(m-1)\hat{\beta}\alpha_m^\infty w_m}{m w_{m-1}} + \phi_{m-1}^{+\infty}(r_p), \tag{A.8}$$

and

$$\alpha_{m+1}^0 = \frac{(m+1)\hat{\beta}\alpha_m^0 a_m}{m a_{m+1}} + \phi_{m+1}^{+0}(r_p), \tag{A.9}$$

$$\alpha_{m+1}^\infty = \frac{(m+1)\hat{\beta}\alpha_m^\infty w_m}{m w_{m+1}} + \phi_{m+1}^{+\infty}(r_p). \tag{A.10}$$

Next, the jump conditions for the derivatives at the sidebands, (31) and (33), are used to produce

$$\frac{a_{m+1}}{a_m} = \frac{\hat{\beta}(m+1)}{m r_p} \frac{\alpha_m^0((m+1)(1+s) + r_p\phi_{m+1}'^-)}{(\phi_{m+1}'^{+0}(r_p) - \phi_{m+1}^{+0}(r_p)\phi_{m+1}'^-(r_p))} \tag{A.11}$$

$$\frac{w_{m+1}}{w_m} = \frac{\hat{\beta}(m+1)}{m r_p} \frac{\alpha_m^\infty((m+1)(1+s) + r_p\phi_{m+1}'^-)}{(\phi_{m+1}'^{+\infty}(r_p) - \phi_{m+1}^{+\infty}(r_p)\phi_{m+1}'^-(r_p))}, \tag{A.12}$$

and

$$\frac{a_{m-1}}{a_m} = \frac{\hat{\beta}(m-1)}{m r_p} \frac{\alpha_m^0(-(m-1)(1+s) + r_p\phi_{m-1}'^-)}{(\phi_{m-1}'^{+0}(r_p) - \phi_{m-1}^{+0}(r_p)\phi_{m-1}'^-(r_p))} \tag{A.13}$$

$$\frac{w_{m-1}}{w_m} = = \frac{\hat{\beta}(m-1)}{m r_p} \frac{\alpha_m^\infty(-(m-1)(1+s) + r_p\phi_{m-1}'^-)}{(\phi_{m-1}'^{+\infty}(r_p) - \phi_{m-1}^{+\infty}(r_p)\phi_{m-1}'^-(r_p))}. \tag{A.14}$$

The main harmonic derivative jump condition, (29), gives

$$r_p(a_m\alpha_{ps}^0\phi'^{ps}(r)(r_p)) = \tag{A.15}$$

$$a_{m+1}m\hat{\beta}\left((1+s)\phi^{+0}_{m+1}(r_p)+\frac{r_p}{(m+1)}\phi'^{+0}_{m+1}(r_p)\right)$$
$$+\,a_{m-1}m\hat{\beta}\left(-(1+s)\phi^{+0}_{m-1}(r_p)+\frac{r_p}{(m-1)}\phi'^{+0}_{m-1}(r_p)\right),$$

and

$$r_p(w_m\alpha^{\infty}_{ps}\phi'^{ps}(r)(r_p)) = \tag{A.16}$$
$$w_{m+1}m\hat{\beta}\left((1+s)\phi^{+\infty}_{m+1}(r_p)+\frac{r_p}{(m+1)}\phi'^{+\infty}_{m+1}(r_p)\right)$$
$$+\,w_{m-1}m\hat{\beta}\left(-(1+s)\phi^{+\infty}_{m-1}(r_p)+\frac{r_p}{(m-1)}\phi'^{+\infty}_{m-1}(r_p)\right).$$

These equations with (A.11) and (A.13) determine

$$\alpha^0_{ps}=\alpha^0_m\hat{\beta}^2(A^0_{m+1}+A^0_{m-1}), \tag{A.17}$$

and with (A.12) and (A.14) determine

$$\alpha^{\infty}_{ps}=\alpha^{\infty}_m\hat{\beta}^2(A^{\infty}_{m+1}+A^{\infty}_{m-1}), \tag{A.18}$$

where

$$A^{0,\infty}_{m+1}=\frac{1}{r_p^2}\left(\frac{((m+1)(1+s)+r_p\phi'^{-}_{m+1})((1+s)(m+1)\phi^{+0,\infty}_{m+1}(r_p)+r_p\phi'^{+0,\infty}_{m+1}(r_p))}{(\phi'^{+0,\infty}_{m+1}(r_p)-\phi^{+0,\infty}_{m+1}(r_p)\phi'^{-}_{m+1}(r_p))}\right),$$
$$A^{0,\infty}_{m-1}=\frac{1}{r_p^2}\left(\frac{(-(m-1)(1+s)+r_p\phi'^{-}_{m-1})(-(1+s)(m-1)\phi^{+0,\infty}_{m-1}(r_p)+r_p\phi'^{+0,\infty}_{m-1}(r_p))}{(\phi'^{+0,\infty}_{m-1}(r_p)-\phi^{+0,\infty}_{m-1}(r_p)\phi'^{-}_{m-1}(r_p))}\right).$$

For compactness $A^{0,\infty}_{m+1}+A^{0,\infty}_{m-1}\equiv f^{0,\infty}$ is defined, so that $\alpha^{0,\infty}_{ps}=\hat{\beta}^2f^{0,\infty}\alpha^{0,\infty}_m$.

Appendix A.5. Form of Δ': no wall and perfect wall

The form of Δ' can now be calculated for the no wall and perfect wall cases. The condition for continuity at the resonant surface gives

$$\alpha^0_m=\frac{\phi^{+0}_m(r_s)}{\phi^{-}_m(r_s)+\hat{\beta}^2\phi^{ps}(r_s)f^0}, \tag{A.19}$$

in the no wall case and in the perfect wall case

$$\alpha^{\infty}_m=\frac{\phi^{+\infty}_m(r_s)}{\phi^{-}_m(r_s)+\hat{\beta}^2\phi^{ps}(r_s)f^{\infty}}. \tag{A.20}$$

The no wall Δ' is calculated from its definition (6) to be

$$\Delta'^0_s=r_s\left(\frac{\phi'^{+0}_m}{\phi^{+0}_m}-\frac{\phi'^{-}_m(r_s)+\phi'^{ps}(r_s)\hat{\beta}^2f^0}{\phi^{-}_m(r_s)+\phi^{ps}(r_s)\hat{\beta}^2f^0}\right)=\frac{e_1+e_2\hat{\beta}^2}{e_3(\hat{\beta}^2-\hat{\beta}^2_{\text{No wall}})}, \tag{A.21}$$

and similarly for the perfect wall

$$\Delta'^{\infty}_s=r_s\left(\frac{\phi'^{+\infty}_m}{\phi^{+\infty}_m}-\frac{\phi'^{-}_m(r_s)+\phi'^{ps}(r_s)\hat{\beta}^2f^{\infty}}{\phi^{-}_m(r_s)+\phi^{ps}(r_s)\hat{\beta}^2f^{\infty}}\right)=\frac{e_4+e_5\hat{\beta}^2}{e_6(\hat{\beta}^2-\hat{\beta}^2_{\text{Perfect wall}})}, \tag{A.22}$$

where e_i are pressure free quantities and the no wall limit is

$$\hat{\beta}^2_{\text{No wall}} = \frac{-\phi^-_m(r_s)}{\phi^{ps}(r_s)f^0}, \tag{A.23}$$

and perfect wall limit is

$$\hat{\beta}^2_{\text{Perfect wall}} = \frac{-\phi^-_m(r_s)}{\phi^{ps}(r_s)f^\infty}. \tag{A.24}$$

Appendix A.6. RWM basis functions

The RWM eigenfunction will be formed by combining sufficient triplet basis functions to satisfy the conditions imposed by the resistive wall. The resistive wall imposes three conditions, one for each harmonic, namely

$$\Delta'_w \equiv \left[\frac{r\psi'_j(r)}{\psi_j(r)}\right]_{r_w} = \gamma\tau_w, \tag{A.25}$$

where $j = m-1, m, m+1$. Four triplet basis functions, each multiplied by an arbitrary constant, will thus be required. The four basis functions will be

$$\boldsymbol{\psi}^0 = \begin{pmatrix} a_{m-1}\psi^0_{m-1} \\ a_m\psi^0_m \\ a_{m+1}\psi^0_{m+1} \end{pmatrix}, \qquad \boldsymbol{\psi}^1 = \begin{pmatrix} b_{m-1}\psi^\infty_{m-1} \\ b_m\psi^0_m \\ b_{m+1}\psi^0_{m+1} \end{pmatrix}, \tag{A.26}$$

$$\boldsymbol{\psi}^2 = \begin{pmatrix} c_{m-1}\psi^0_{m-1} \\ c_m\psi^\infty_m \\ c_{m+1}\psi^0_{m+1} \end{pmatrix}, \qquad \boldsymbol{\psi}^3 = \begin{pmatrix} d_{m-1}\psi^0_{m-1} \\ d_m\psi^0_m \\ d_{m+1}\psi^\infty_{m+1} \end{pmatrix}, \tag{A.27}$$

where the values a_i, b_i, c_i, d_i are determined using the pressure step jump conditions as for the no wall and perfect wall cases. One of these basis functions $\boldsymbol{\psi}^0$ is completely physical the other three are non-physical, representing a wall which is perfect to one harmonic but unseen by the others. The coefficients are calculated to be

$$\frac{a_{m-1}}{a_m} = \frac{\hat{\beta}(m-1)}{mr_p}\frac{\alpha^a_m(-(m-1)(s+1) + r_p\phi'^-_{m-1}(r_p))}{(\phi'^{+0}_{m-1}(r_p) - \phi^{+0}_{m-1}(r_p)\phi'^-_{m-1}(r_p))}, \tag{A.28}$$

$$\frac{a_{m+1}}{a_m} = \frac{\hat{\beta}(m+1)}{mr_p}\frac{\alpha^a_m((m+1)(s+1) + r_p\phi'^-_{m+1}(r_p))}{(\phi'^{+0}_{m+1}(r_p) - \phi^{+0}_{m+1}(r_p)\phi'^-_{m+1}(r_p))}, \tag{A.29}$$

where

$$\alpha^a_m = \frac{\phi^{+0}_m(r_s)}{\phi^-_m(r_s) + \hat{\beta}^2\phi^{ps}(r_s)(A^0_{m+1} + A^0_{m-1})}, \tag{A.30}$$

and

$$\frac{b_{m-1}}{b_m} = \frac{\hat{\beta}(m-1)}{mr_p}\frac{\alpha^b_m(-(m-1)(s+1) + r_p\phi'^-_{m-1}(r_p))}{(\phi'^{+\infty}_{m-1}(r_p) - \phi^{+\infty}_{m-1}(r_p)\phi'^-_{m-1}(r_p))}, \tag{A.31}$$

$$\frac{b_{m+1}}{b_m} = \frac{\hat{\beta}(m+1)}{mr_p}\frac{\alpha^b_m((m+1)(s+1) + r_p\phi'^-_{m+1}(r_p))}{(\phi'^{+0}_{m+1}(r_p) - \phi^{+0}_{m+1}(r_p)\phi'^-_{m+1}(r_p))}, \tag{A.32}$$

where

$$\alpha_m^b = \frac{\phi_m^{+0}(r_s)}{\phi_m^-(r_s) + \hat{\beta}^2\phi^{ps}(r_s)(A_{m+1}^0 + A_{m-1}^\infty)}, \tag{A.33}$$

and

$$\frac{c_{m-1}}{c_m} = \frac{\hat{\beta}(m-1)}{mr_p}\frac{\alpha_m^c(-(m-1)(s+1) + r_p\phi'^-_{m-1}(r_p))}{(\phi'^{+0}_{m-1}(r_p) - \phi^{+0}_{m-1}(r_p)\phi'^-_{m-1}(r_p))}, \tag{A.34}$$

$$\frac{c_{m+1}}{c_m} = \frac{\hat{\beta}(m+1)}{mr_p}\frac{\alpha_m^c((m+1)(s+1) + r_p\phi'^-_{m+1}(r_p))}{(\phi'^{+0}_{m+1}(r_p) - \phi^{+0}_{m+1}(r_p)\phi'^-_{m+1}(r_p))}, \tag{A.35}$$

where

$$\alpha_m^c = \frac{\phi_m^{+\infty}(r_s)}{\phi_m^-(r_s) + \hat{\beta}^2\phi^{ps}(r_s)(A_{m+1}^0 + A_{m-1}^0)}, \tag{A.36}$$

and

$$\frac{d_{m-1}}{d_m} = \frac{\hat{\beta}(m-1)}{mr_p}\frac{\alpha_m^d(-(m-1)(s+1) + r_p\phi'^-_{m-1}(r_p))}{(\phi'^{+0}_{m-1}(r_p) - \phi^{+0}_{m-1}(r_p)\phi'^-_{m-1}(r_p))}, \tag{A.37}$$

$$\frac{d_{m+1}}{d_m} = \frac{\hat{\beta}(m+1)}{mr_p}\frac{\alpha_m^d((m+1)(s+1) + r_p\phi'^-_{m+1}(r_p))}{(\phi'^{+\infty}_{m+1}(r_p) - \phi^{+\infty}_{m+1}(r_p)\phi'^-_{m+1}(r_p))}, \tag{A.38}$$

where

$$\alpha_m^d = \frac{\phi_m^{+0}(r_s)}{\phi_m^-(r_s) + \hat{\beta}^2\phi^{ps}(r_s)(A_{m+1}^\infty + A_{m-1}^0)}. \tag{A.39}$$

The total resistive wall eigenfunction will be a combination of these functions

$$\boldsymbol{\psi}^{\mathrm{RWM}} = a_{\mathrm{RWM}}\boldsymbol{\psi}^0 + b_{\mathrm{RWM}}\boldsymbol{\psi}^1 + c_{\mathrm{RWM}}\boldsymbol{\psi}^2 + d_{\mathrm{RWM}}\boldsymbol{\psi}^3. \tag{A.40}$$

It should be noted that since each of these triplet basis functions satisfies the pressure step jump conditions individually, a linear combination of triplet basis functions will also satisfy the pressure step jump conditions.

The three conditions from (A.25) yield the following system of equations

$$b_{\mathrm{RWM}}\frac{b_{m-1}}{b_m} = \gamma\tau_w(a_{\mathrm{RWM}}\frac{a_{m-1}}{a_m} + c_{\mathrm{RWM}}\frac{c_{m-1}}{c_m} + d_{\mathrm{RWM}}\frac{d_{m-1}}{d_m}), \tag{A.41}$$

$$c_{\mathrm{RWM}} = \gamma\tau_w(a_{\mathrm{RWM}} + b_{\mathrm{RWM}} + d_{\mathrm{RWM}}), \tag{A.42}$$

$$d_{\mathrm{RWM}}\frac{d_{m+1}}{d_m} = \gamma\tau_w(a_{\mathrm{RWM}}\frac{a_{m+1}}{a_m} + b_{\mathrm{RWM}}\frac{b_{m+1}}{b_m} + c_{\mathrm{RWM}}\frac{c_{m+1}}{c_m}). \tag{A.43}$$

The solution of this system of equations is

$$\begin{aligned} a_{\mathrm{RWM}} = & -1 + \left(\frac{\alpha_m^c}{\alpha_m^d}g_{m+1} + g_{m+1}g_{m-1} + \frac{\alpha_m^c}{\alpha_m^b}g_{m-1}\right)(\gamma\tau_w)^2 \\ & + \left(\frac{\alpha_m^c}{\alpha_m^d}g_{m+1}g_{m-1} + \frac{\alpha_m^c}{\alpha_m^b}g_{m+1}g_{m-1}\right)(\gamma\tau_w)^3, \end{aligned} \tag{A.44}$$

$$\begin{aligned} b_{\mathrm{RWM}} = & -(\gamma\tau_w)\left(\frac{\alpha_m^a}{\alpha_m^b}g_{m-1} + (\gamma\tau_w)\left(\frac{\alpha_m^c}{\alpha_m^b}g_{m-1} + \frac{\alpha_m^a}{\alpha_m^b}g_{m+1}g_{m-1}\right)\right. \\ & \left. + (\gamma\tau_w)^2\left(\frac{\alpha_m^c}{\alpha_m^b}g_{m+1}g_{m-1}\right)\right), \end{aligned} \tag{A.45}$$

$$c_{\rm RWM} = -(\gamma\tau_w)\left(1+(\gamma\tau_w)\left(\frac{\alpha_m^a}{\alpha_m^d}g_{m+1}+\frac{\alpha_m^a}{\alpha_m^b}g_{m-1}\right)\right. \tag{A.46}$$
$$\left. + \ (\gamma\tau_w)^2 g_{m+1}g_{m-1}\left(\frac{\alpha_m^a}{\alpha_m^b}-1+\frac{\alpha_m^a}{\alpha_m^d}\right)\right),$$

$$d_{\rm RWM} = -(\gamma\tau_w)\left(\frac{\alpha_m^a}{\alpha_m^d}g_{m+1}+(\gamma\tau_w)\left(\frac{\alpha_m^a}{\alpha_m^d}g_{m+1}g_{m-1}+\frac{\alpha_m^c}{\alpha_m^d}g_{m+1}\right)\right. \tag{A.47}$$
$$\left. + \ (\gamma\tau_w)^2\left(\frac{\alpha_m^c}{\alpha_m^d}g_{m+1}g_{m-1}\right)\right),$$

where

$$g_{m+1} = \frac{(\phi_{m+1}'^{+\infty}(r_p) - \phi_{m+1}^{+\infty}(r_p)\phi_{m+1}'^{-}(r_p)}{(\phi_{m+1}'^{+0}(r_p) - \phi_{m+1}^{+0}(r_p)\phi_{m+1}'^{-}(r_p)}, \tag{A.48}$$

$$g_{m-1} = \frac{(\phi_{m-1}'^{+\infty}(r_p) - \phi_{m-1}^{+\infty}(r_p)\phi_{m-1}'^{-}(r_p)}{(\phi_{m-1}'^{+0}(r_p) - \phi_{m-1}^{+0}(r_p)\phi_{m-1}'^{-}(r_p)}. \tag{A.49}$$

Appendix A.7. Form of Δ' for the pressure driven kink mode

Using the definition (16) in this case gives

$$\Delta_s' = r_s\frac{a_{\rm RWM}[\psi_m'^0]_{r_s} + b_{\rm RWM}[\psi_m'^1]_{r_s} + c_{\rm RWM}[\psi_m'^2]_{r_s} + d_{\rm RWM}[\psi_m'^3]_{r_s}}{a_{\rm RWM}\phi_m^{+0}(r_s) + b_{\rm RWM}\phi_m^{+0}(r_s) + c_{\rm RWM}\phi_m^{+\infty}(r_s) + d_{\rm RWM}\phi_m^{+0}(r_s)}, \tag{A.50}$$

where

$$\begin{aligned}
\left[\psi_m^0\right]_{r_s} &= \phi_m'^{+0} - \alpha_m^a(\phi_m'^{-} + \hat\beta^2\phi'^{ps}(A_{m+1}^0 + A_{m-1}^0))\\
\left[\psi_m^1\right] &= \phi_m'^{+0} - \alpha_m^b(\phi_m'^{-} + \hat\beta^2\phi'^{ps}(A_{m+1}^0 + A_{m-1}^\infty))\\
\left[\psi_m^2\right]_{r_s} &= \phi_m'^{+\infty} - \alpha_m^c(\phi_m'^{-} + \hat\beta^2\phi'^{ps}(A_{m+1}^0 + A_{m-1}^0))\\
\left[\psi_m^3\right]_{r_s} &= \phi_m'^{+0} - \alpha_m^d(\phi_m'^{-} + \hat\beta^2\phi'^{ps}(A_{m+1}^\infty + A_{m-1}^0))
\end{aligned}$$

The final form of Δ' is thus

$$\Delta_s' = \frac{a_0 + a_1\gamma\tau_w + a_2(\gamma\tau_w)^2 + a_3(\gamma\tau_w)^3}{b_0 + b_1\gamma\tau_w + b_2(\gamma\tau_w)^2 + b_3(\gamma\tau_w)^3}, \tag{A.51}$$

where the a_i, b_i are pressure dependent, as given in (36).

A Taylor expansion with the normalization of ϕ^{ps} gives

$$\phi^{ps}(r_s) = \phi^{ps}(r_p+\delta r) \approx \phi^{ps}(r_p) + \delta r\phi'^{ps}(r_p) = \delta r, \tag{A.52}$$

where $\delta r = r_s - r_p$. The magnetic shear is defined as $s = (r/q)q'$ so that

$$\delta r \approx \frac{r}{sq}\delta q, \tag{A.53}$$

where $\delta q = q(r_s) - q(r_p)$. Finally,

$$\kappa \equiv m - nq(r_p) = nq(r_s) - nq(r_p) = n\delta q, \tag{A.54}$$

gives

$$\phi^{ps}(r_s) \approx \frac{r_p\kappa}{ns(r_p)q(r_p)}, \tag{A.55}$$

and using a similar argument, $\phi'^{ps}(r_s) \sim 1 + O(\kappa)$.

Appendix A.8. Form of Δ' for the current driven kink mode

The calculation of Δ' for the current driven kink mode is simpler than for the pressure driven kink mode. The lower $\hat{\beta}$ ordering implies that $r_s \approx r_p$ so that $\phi^{ps}(r_s) \approx \phi^{ps}(r_p) = 0$ and $\phi'^{ps}(r_s) \approx \phi'^{ps}(r_p) = 1$. Using these expressions it can be shown that

$$\begin{aligned}
a_{\rm RWM} =& -1 + (\gamma\tau_w)^2 \left(\frac{\phi_m^{+\infty}}{\phi_m^{+0}} g_{m+1} g_{m-1}\right) \left(\frac{1}{g_{m-1}} + \frac{\phi_m^{+0}(r_s)}{\phi_m^{+\infty}(r_s)} + \frac{1}{g_{m-1}} + 2(\gamma\tau_w)\right), \\
b_{\rm RWM} =& -(\gamma\tau_w) \frac{\phi_m^{+0}(r_s)}{\phi_m^{+\infty}(r_s)} g_{m+1} g_{m-1} \\
& \times \left(\frac{\phi_m^{+\infty}(r_s)}{\phi_m^{+0}(r_s)} \frac{1}{g_{m+1}} + (\gamma\tau_w) \left(\frac{1}{g_{m+1}} + \frac{\phi_m^{+\infty}(r_s)}{\phi_m^{+0}(r_s)}\right) + (\gamma\tau_w)^2\right) \\
c_{\rm RWM} =& -(\gamma\tau_w) \left(1 + (\gamma\tau_w)\left(g_{m+1} + g_{m-1}\right) + (\gamma\tau_w)^2 g_{m+1} g_{m-1}\right), \\
d_{\rm RWM} =& -(\gamma\tau_w) \left(g_{m+1} + (\gamma\tau_w) \left(g_{m+1} g_{m-1} + \frac{\phi_m^{+\infty}}{\phi_m^{+0}} g_{m+1}\right)\right. \\
& + \left.(\gamma\tau_w)^2 \left(\frac{\phi_m^{+\infty}}{\phi_m^{+0}} g_{m+1} g_{m-1}\right)\right),
\end{aligned}$$

and also that

$$\alpha_m^a = \alpha_m^b = \alpha_m^d = \frac{\phi_m^{+0}(r_s)}{\phi_m^-(r_s)}, \qquad \text{and} \qquad \alpha_m^c = \frac{\phi_m^{+\infty}(r_s)}{\phi_m^-(r_s)}. \tag{A.56}$$

The final form of the stability index for the current driven kink mode is thus

$$\Delta'_s = \frac{c_0 + \gamma\tau_w c_1 + (\gamma\tau_w)^2 c_2 + (\gamma\tau_w)^3 c_3 + \hat{\beta}^2 (d_0 + \gamma\tau_w d_1 + (\gamma\tau_w)^2 d_2 + (\gamma\tau_w)^3 d_3)}{a_0 + \gamma\tau_w a_1 + (\gamma\tau_w)^2 a_2 + (\gamma\tau_w)^3 a_3}, \tag{A.57}$$

where a_i, c_i and d_i are pressure free constants depending on the equilibrium, as given in (35).

References

[1] Aymar R, Barabaschi P, and Shimomura Y 2002 *Plasma Phys. Control. Fusion* **44** 519
[2] Reimerdes H *et al.* 2006 *Phys. Plasmas* **13** 056107
[3] Hender T C *et al.* 2007 *Nucl. Fusion* **47** S128–S202
[4] Reimerdes H *et al.* 2007 *Plasma Phys. Control. Fusion* **49** B349
[5] Finn J M 1995 *Phys. Plasmas* **2** 198
[6] Finn J M 1995 *Phys. Plasmas* **2** 3782
[7] Bondeson A and Xie H X 1997 *Phys. Plasmas* **4** 2081
[8] Bondeson A and Ward D J 1994 *Phys. Rev. Lett.* **72** 2709
[9] Betti R and Freidberg J P 1995 *Phys. Rev. Lett.* **74** 2949
[10] Bondeson A and Chu M S 1996 *Phys. Plasmas* **3** 3013
[11] Hu B and Betti R 2004 *Phys. Rev. Let.* **93** 105002
[12] Gimblett C G and Hastie R J 1998 *Proceedings of the Joint Varenna-Lausanne International Workshop on the Theory of Fusion Plasmas, Varenna 31 August - 4th September 1998.* (Editrice Compositori, Bologna) p 319
[13] Zheng L J, Kotschenreuther M, and Chu M S 2005 *Phys. Rev. Lett.* **95** 255003
[14] Liu Y Q *et al.* 2009 *Phys. Plasmas* **16** 056113

[15] Betti R 1998 *Phys. Plasmas* **5** 3615
[16] Connor J W *et al.* 1988 *Phys. Fluids* **31** 577
[17] Porcelli F 1987 *Phys. Fluids* **30** 1734
[18] Gimblett C G 1986 *Nuclear Fusion* **26** 617
[19] Newcomb W A 1960 *Ann. Phys.* **10** 232
[20] Ham C J, Gimblett C G, and Hastie R J 2009 *Plasma Phys. Control. Fusion* **51** 115010
[21] Freidberg J P 1987 *Ideal Magnetohydrodynamics* (New York: Plenum Press)
[22] Glasser A H, Greene J M and Johnson J L 1976 *Phys. Fluids* **19** 567
[23] Mikhailovskii A B and Tsypin V S 1983 *Sov. J. Plasma Phys.* **9** 91
[24] Rosenbluth M N and Hinton F L 1998 *Phys. Rev. Lett.* **80** 724
[25] Hinton F L and Robertson J A 1984 *Phys. Fluids* **27** 1243
[26] Shaing K C 2004 *Phys. PLasmas* **11** 5525
[27] Fitzpatrick R and Aydemir A Y 1996 *Nucl. Fusion* **36** 11
[28] Lighthill M J 1958 *Introduction to Fourier Analysis and Generalized Functions* (Cambridge: Cambridge University Press)
[29] Connor J W, Hastie R J and Taylor J B 1978 *Phys. Rev. Lett.* **40** 396
[30] Martin T J, Connor J W, and Hastie R J 1991 AEA Fusion Report, AEA FUS 91.
[31] Allfrey S J *et al.* 1998 *Proceedings of the 25th EPS Conference on Controlled Fusion and Plasma Physics, Prague* edited by P Pavlov (European Physical Society, Petit-Lancy) ECA **22C** p 2026-2029
[32] Wesson J 1997 *Tokamaks* (Oxford: Oxford University Press)
[33] Takechi M *et al.* 2007 *Phys. Rev. Lett.* **98** 055002
[34] Bondeson A *et al.* 2003 *Plasma Phys. Control. Fusion* **45** A253